21st Australasian Fluid Mechanics Conference
Adelaide, Australia
10-13 December 2018

Towards closure relations for the rise velocity of Taylor bubbles in annular piping using phase-field lattice Boltzmann techniques

T. R. Mitchell[1], C. R. Leonardi[1], M. Firouzi[2] and B. F. Towler[2]

[1]School of Mechanical and Mining Engineering
The University of Queensland, St. Lucia, Queensland 4072, Australia

[2]School of Chemical Engineering
The University of Queensland, St. Lucia, Queensland 4072, Australia

Abstract

Two-phase slug flow is a common phenomenon observed in oil and gas wells and pipelines. Mechanistic modelling approaches used in industry for design and monitoring rely on closure relations (e.g. Taylor bubble rise velocity in a stagnant fluid) to approximate phase interactions. In this work, the phase-field lattice Boltzmann method (PFLBM) originally proposed by Fakhari *et al.* [4] and extended to three dimensions by Mitchell *et al.* [10] is employed to investigate the validity of some of these closure relations. The PFLBM solves the conservative phase-field equation to capture the interfacial dynamics while resolving the hydrodynamics through a velocity-evolution LBM. To assist with model stability at high density and viscosity ratios, a weighted-multiple-relaxation-time (WMRT) operator is incorporated in the hydrodynamic scheme. The model is first validated for Taylor bubble transport in vertical pipes at a range of Morton (Mo) and Eötvös (Eo) numbers. The effect of inclination in tubular pipes is then investigated and compared with existing correlations in the literature. The study concludes with an assessment of the Taylor bubble rise velocity in annular piping with comparison to experimental results.

Themes: Computational fluid dynamics; Multiphase and particle-laden flows; Pipe flows.

Introduction

Multiphase flows are prevalent in a number of industrial, natural and scientifically-relevant problems. The complexities of such flows present a number of challenges in the oil and gas industry, where two- and three-phase confined flows are commonplace. The development of characteristic interface topologies, referred to as flow regimes, is often observed in the transport of hydrocarbons from subsurface reservoirs. In order to accurately predict system performance and then adequately design and operate fluid handling and pressure management systems, it is important to understand both when a regime will occur and the associated dynamics. A comprehensive review of the relevant flow regimes can be found in Wu *et al.* [15].

When relating multiphase flows to general formulae, it is important to assign relevant dimensionless numbers. In situations where the density and viscosity ratios are high, one can relate the propagation of a Taylor bubble through five non-dimensional groups [8]. The numbers commonly used for this include the Froude number, $\mathrm{Fr} = u_{TB}/\sqrt{gD}$, the Eötvös number, $\mathrm{Eo} = g\rho D^2/\sigma$, the Morton number, $\mathrm{Mo} = g\mu^4/\rho\sigma^3$, the liquid Reynolds number, $\mathrm{Re} = \rho u_l D/\mu$, and the pipe angle, θ. In this work, we also refer to the inverse viscosity number, $\mathrm{Nf} = \rho\sqrt{gD^3}/\mu$.

Governing equations

In this work, a one-fluid approach is used to simulate Taylor bubble dynamics through various piping configurations. This means that the fluid behaviour is captured through a single set of continuity relations with variable material properties. The material properties, namely density and viscosity, are described by an order parameter (commonly related to the fluid volume fraction) which is propagated throughout the flow via an interface tracking method (ITM). Various ITMs exist in the literature, including the Volume-of-Fluid and Level-Set methods, however in this study the conservative phase field model (PFM) is used. This particular PFM was proposed as a modified Allen-Cahn equation, before being formulated in a conservative form. Geier *et al.* [5] presented the model within the lattice Boltzmann framework and were able to show mass conservation and robust model behaviour over a range of test cases. The order parameter, ϕ, takes two extreme values in the low density, ϕ_L, and high density, ϕ_H, phases. The explicit location of the interface is then taken to be the level set curved defined by the average of these two values, $\phi = \phi_0 = 0.5(\phi_\mathrm{L} + \phi_\mathrm{H})$. The equation then governing the dynamics of this parameter field is given by Chiu and Lin [2] as,

$$\partial_t \phi + \boldsymbol{\nabla}\cdot\phi\boldsymbol{u} = \boldsymbol{\nabla}\cdot M\left(\boldsymbol{\nabla}\phi - \frac{\boldsymbol{\nabla}\phi}{|\boldsymbol{\nabla}\phi|}\frac{1-4(\phi-\phi_0)^2}{\xi}\right), \qquad (1)$$

where $\boldsymbol{u}$ is the velocity vector, M is the mobility, and ξ describes the diffuse interfacial width. It is assumed that the profile of ϕ over the diffuse interface varies as,

$$\phi(\boldsymbol{x}) = \phi_0 \pm \frac{\phi_\mathrm{H}-\phi_\mathrm{L}}{2}\tanh\left(\frac{2|\boldsymbol{x}-\boldsymbol{x}_0|}{\xi}\right), \qquad (2)$$

where $\boldsymbol{x_0}$ is the coordinate position indicating the interface location. The density, ρ, and dynamic viscosity, μ, are recovered by a simple linear interpolation using ϕ.

The hydrodynamics of the system is governed through the incompressible continuity and momentum equations given by,

$$\partial_t \rho + \boldsymbol{\nabla}\cdot\rho\boldsymbol{u} = 0, \qquad (3)$$

$$\rho\left(\partial_t\boldsymbol{u} + \boldsymbol{u}\cdot\boldsymbol{\nabla}\boldsymbol{u}\right) = -\boldsymbol{\nabla}p + \boldsymbol{\nabla}\cdot\Pi + \rho\boldsymbol{g} + \mathbf{F}_\mathrm{s}, \qquad (4)$$

where p is the hydrodynamic pressure, $\Pi = \mu\left[\boldsymbol{\nabla}\boldsymbol{u} + (\boldsymbol{\nabla}\boldsymbol{u})^T\right]$ is the viscous stress tensor, $\boldsymbol{g}$ is the gravitational acceleration and $\mathbf{F}_\mathrm{s} = \mu_\phi\boldsymbol{\nabla}\phi$ is the force associated with the surface tension, with,

$$\mu_\phi = 4\beta(\phi-\phi_\mathrm{L})(\phi-\phi_\mathrm{H})(\phi-\phi_0) - \kappa\nabla^2\phi. \qquad (5)$$

Here, μ_ϕ is the chemical potential and relations to the surface tension, σ, and interfacial width are introduced through $\beta = 12\sigma/\xi$ and $\kappa = 3\sigma\xi/2$.

Lattice Boltzmann formulation

The discretisation of the governing equations is conducted as per the work of Fakhari *et al.* [4] and Mitchell *et al.* [10],

to which the reader is referred for detailed descriptions of the model. Equation 1 is resolved in the lattice Boltzmann framework using a single-relaxation-time collision operator on a D3Q15 lattice. The explicit update equation for this is,

$$h_i(\boldsymbol{x}+\boldsymbol{c}_i\delta t, t+\delta t) = h_i(\boldsymbol{x},t) - \frac{h_i(\boldsymbol{x},t)-\bar{h}_i^{\mathrm{eq}}(\boldsymbol{x},t)}{\tau_\phi + 1/2} + F_i^\phi(\boldsymbol{x},t), \tag{6}$$

where $\tau_\phi = M/c_s^2$ is the phase-field relaxation time and $c_s = c/\sqrt{3}$ is the speed of sound of the system. The forcing term is then given by,

$$F_i^\phi(\boldsymbol{x},t) = \delta t \frac{[1-4(\phi-\phi_0)^2]}{\xi} w_i \boldsymbol{c}_i \cdot \frac{\boldsymbol{\nabla}\phi}{|\boldsymbol{\nabla}\phi|}, \tag{7}$$

where $\boldsymbol{c}_i$ is the discrete velocity set and w_i represents the weights of the lattice. The equilibrium distribution used in the update equation is shifted by the forcing term,

$$\bar{h}_i^{\mathrm{eq}}(\boldsymbol{x},t) = \phi w_i \left(1 + \frac{\boldsymbol{c}_i\cdot\boldsymbol{u}}{c_s^2} + \frac{(\boldsymbol{c}_i\cdot\boldsymbol{u})^2}{2c_s^4} - \frac{\boldsymbol{u}\cdot\boldsymbol{u}}{2c_s^2}\right) - \frac{1}{2}F_i^\phi. \tag{8}$$

To relate the interface-tracking distribution function, h_i, to the phase-field variable, its zeroth moment, $\phi = \sum_i h_i$, is taken after the streaming step.

To resolve the hydrodynamics of the system, the weighted-multiple-relaxation-time collision operator is used on a D3Q27 lattice. The lattice Boltzmann equation as defined in Mitchell *et al.* [10] is,

$$\begin{aligned} g_i(\boldsymbol{x}+\boldsymbol{c}_i\delta t, t+\delta t) =& g_i(\boldsymbol{x},t) \\ &- \mathbf{M}^{-1}\hat{\mathbf{S}}\mathbf{M}\left[g_i(\boldsymbol{x},t) - \bar{g}_i^{\mathrm{eq}}(\boldsymbol{x},t)\right] + F_i(\mathbf{x},t), \end{aligned} \tag{9}$$

where the shifted equilibrium distribution is,

$$\bar{g}_i^{\mathrm{eq}}(\boldsymbol{x},t) = w_i\left[\frac{p}{\rho c_s^2} + \left(\frac{\boldsymbol{c}_i\cdot\boldsymbol{u}}{c_s^2} + \frac{(\boldsymbol{c}_i\cdot\boldsymbol{u})^2}{2c_s^4} - \frac{\boldsymbol{u}\cdot\boldsymbol{u}}{2c_s^2}\right)\right] - \frac{1}{2}F_i. \tag{10}$$

Here, it is noted that the initialisation process involves setting the domain equal to the equilibrium distribution functions. The collision matrix, $\mathbf{M}$, and relaxation matrix, $\hat{\mathbf{S}}$, are listed in Mitchell *et al.* [10]. Here, this work improves the efficiency of the algorithm by incorporating the forcing term within momentum space (i.e. prior to applying the $\mathbf{M}^{-1}$ transformation). The procedure for doing this involves first calculating the total volumetric force, $\mathbf{F} = \rho\boldsymbol{g} + \mathbf{F}_\mathrm{s} + \mathbf{F}_\mathrm{p} + \mathbf{F}_\mu$, where $\mathbf{F}_\mathrm{p}$ and $\mathbf{F}_\mu$ are introduced to recover the pressure and viscous terms within the Navier-Stokes equation. The pressure force is given by,

$$\mathbf{F}_\mathrm{p} = -\frac{p}{\rho}(\rho_\mathrm{H} - \rho_\mathrm{L})\boldsymbol{\nabla}\phi, \tag{11}$$

and the viscous force as [4],

$$\mathbf{F}_\mu = \nu(\rho_\mathrm{H} - \rho_\mathrm{L})\left[\boldsymbol{\nabla}\boldsymbol{u} + (\boldsymbol{\nabla}\boldsymbol{u})^T\right]\cdot\boldsymbol{\nabla}\phi, \tag{12}$$

wherein the derivatives of the order parameter are recovered with isotropic central differences. The velocity derivatives can be obtained from the second moment of the hydrodynamic distribution function,

$$F_{\mu,\alpha} = -\frac{\nu(\rho_\mathrm{H}-\rho_\mathrm{L})}{c_s^2}\left[\sum_i c_{i,\alpha}c_{i,\beta}\sum_j(\mathbf{M}^{-1}\hat{\mathbf{S}}\mathbf{M})_{i,j}(g_i - g_i^{\mathrm{eq}})\right]\partial_\beta\phi. \tag{13}$$

Therefore, defining the moments, $\boldsymbol{m} = \mathbf{M}\boldsymbol{g}$, and the forcing term, $\mathbf{F}_\mathbf{m} = \rho^{-1}(0, F_x, F_y, F_z, 0, \ldots, 0)$, such that it acts on the correct moments, the update can be performed as,

$$g_i(\boldsymbol{x}+\boldsymbol{c}_i\delta t, t+\delta t) = \mathbf{M}^{-1}\left[m_i - (m_i - m_i^{eq} + 0.5F_{m,i})\hat{S}_{i,i} + F_{m,i}\right]. \tag{14}$$

The simplifications that arise from performing the update in this form was found to approximately halve the required computation time, which we have observed to scale while the compute rather than communication is the limiting factor. The macroscopic properties recovered from the hydrodynamic distribution function, g_i, are the pressure, $p = \rho c_s^2\sum_i g_i$, and velocity, $\boldsymbol{u} = \sum_i g_i\boldsymbol{c}_i + \mathbf{F}/2\rho$.

Taylor bubble tubular simulations

To demostrate the robustness of the described lattice Boltzmann model, a number of cases from a numerical study conducted in the finite volume software TransAT® [8] were analysed. Table 1 indicates the test matrix, where cases are defined based on their Mo, Eo and Nf numbers. The experimental fluid properties were not captured in the simulations. Instead, a density and dynamic viscosity ratio of 1000 was defined, enforcing $\rho_\mathrm{L} \ll \rho_\mathrm{H}$ and $\mu_\mathrm{L} \ll \mu_\mathrm{H}$. The discretised domain consisted of 128 lattice cells across the tube diameter, D, and the length of the tube was set to $10D$. The bounceback method was used to create no-slip pipe walls as well as to close the top and bottom of the domain. In the simulations, a reference time, $t_0 = \sqrt{D/g} = 12000$ lattice units, is defined such that $t^* = t/t_0$ is the dimensionless time. Simulations are run for $10t^*$ at which time the Taylor bubbles have progressed towards a steady-state nose and film profile as well as a macroscopic rise velocity.

Table 1 displays the results for the bubble Froude number and the dimensionless developed film thickness, $h^* = h/R$, where h is the distance of the interface from the tube wall and R is the tube radius. Four of the eight test cases were compared with experimentally obtained rise velocities as well as the work of Lizarraga-Garcia *et al.* [8], which developed an advanced, unified correlation for Taylor bubble rise that agreed well with a large database of results. This made it a reputable source for comparison. Case C comes from the work of Shosho and Ryan

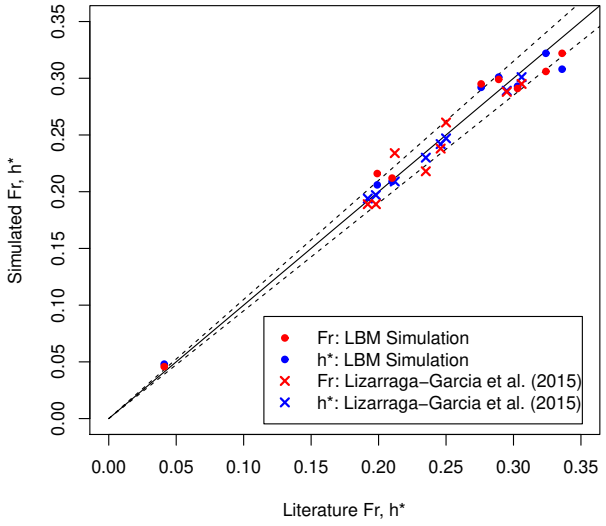

Figure 1: Comparison of the (a) Froude number and (b) dimensionless film thickness for the simulated Taylor bubble with those expected from the literature. The solid line indicates a perfect match with literature and dashed lines show ±5%.

Table 1: Summary of Taylor bubble rise and film thickness over a range of Eo and Nf numbers in comparison with literature and the finite volume method (FVM) simulations of Lizarraga-Garcia *et al.* [8]. Experimental results are highlighted with an asterisk (*).

Case	Mo	Eo	Nf	Fr (lit.)	Fr (FVM)	Fr (LBM)	h^* (lit.)	h^* (FVM)	h^* (LBM)
A	0.328	76.5	34.2	0.210	0.212	0.209	0.295	0.288	0.289
B	4.03e-3	187	201	0.324	0.306	0.322	0.198	0.189	0.197
C	1.17e-4	38.6	149	0.276*	0.295	0.292	0.212	0.234	0.209
D	1.52e-2	98.4	89.0	0.303*	0.291	0.293	0.246*	0.238	0.242
E	1.50e-3	9.88	82.3	0.0411	0.0458	0.048	0.192	0.189	0.194
F	4.75e-2	192	111	0.336*	0.322	0.308	0.235*	0.218	0.230
G	8.38	747	84.0	0.289*	0.299	0.301	0.250	0.261	0.247
H	8.38	181	29.0	0.199	0.216	0.206	0.306	0.295	0.301

[13]; case D from Bugg and Saad [1]; case F from Nogueira *et al.* [11]; and case G from Jeyachandra *et al.* [7], whereas the remaining cases were compared with the literature correlation from Viana *et al.* [14]. In terms of the developed film thickness, two experimental cases reported values for this (Cases D and F), while the remainder were compared to the Cubic Brown model proposed by Llewellin *et al.* [9].

The results from Table 1 are displayed graphically in Figure 1. These plots indicate the deviation of the simulation results, using both the LBM described here and the finite volume method [8], from results reported in the literature. To quantify this, the average absolute difference was calculated in which the phase field LBM was able to capture the rise behaviour of the Taylor bubble, as indicated by the Froude number, to approximately $\pm 5.4\%$. The dimensionless film thickness was found to be on average $\pm 1.4\%$ of the expected value. The simulations conducted here indicate both the robustness of the multiphase lattice Boltzmann model, as well as the accuracy of correlations existing for vertical tubes.

Effect of pipe inclination

To determine the effect of pipe inclination, the test cases conducted by Lizarraga-Garcia *et al.* [8] were studied at a wider range of rotations. Here, Cases A and G were analysed at inclinations of $\theta = (5, 15, 30, 45, \ldots, 90)$ degrees from horizontal. The present results were compared to a range of correlations [6, 7, 12]. In addition, Case G was also compared with experimental data [7].

Figure 2 shows excellent agreement between the LBM test conducted in this study and the available range of numerical results [8]. This is evident over a large range of angles in Figure 2. In Figure 2b it can be seen that the LBM results very accurately capture the experimental work of Jeyachandra *et al.* [7]. From these findings, it is evident that the existing correlations in the literature are inadequate to capture the rise velocity of Taylor bubbles over both a range of inclination angles and fluid properties. Arguably, the most accuate correlation overall, as pointed out by [8], was that of Hasan *et al.* [6]. It is noted that the original correlation has been modified slightly, namely from a constant value of $Fr_d^v = 0.35$ to,

$$Fr_d = Fr_d^v \sqrt{sin(\theta)}(1 + cos(\theta))^{1.2}, \tag{15}$$

$$Fr_d^v = \frac{0.34}{(1 + 3805/\mathrm{Eo}^{3.06})^{0.58}}. \tag{16}$$

Equation 16 was proposed by Viana *et al.* [14] to account for the effects of surface tension and viscous forces.

Annular pipe configuration

Having shown the capability and robustness of the presented phase field LBM, a preliminary study on the flow of Taylor bubbles in annular pipes was conducted. This was performed in comparison with the experimental work of Das *et al.* [3]. Here the equivalent Froude number for the bubble is defined based on the summation of the inner, d_1, and outer, d_2, diameters, $Fr_a = U_{TB}/\sqrt{g(d_1 + d_2)}$. Simulations were conducted with the same resolution as the tubular flow cases, however, the reference time was reduced to $t_0 = 5000$ in order to lower computational run time. The sensitivity of this parameter is still to be investigated. The reported experimental work was conducted with air and water as the working fluids, as such the density ratio was set to 828 and the dynamic viscosity ratio to 55.

Table 2 provides a summary of the experimental geometry, the relevant dimensionless numbers as well as the rise velocity results. The predicted Fr number was that defined by the group of Das *et al.* [3], where it is seen to very accurately capture the measurements conducted by the same group. The results obtained in the current work show deviation from these measured values. However, the level of variance is still a considerable reduction on the deviation Das *et al.* [3] reported with correlations from other authors.

Table 2: Summary of annular experimental geometry and flow cases from Das *et al.* [3]. The error presented is variation between measured results and lattice Boltzmann simulations.

Case	d_1 [m]	d_2 [m]	Eo	Mo
1	0.0508	0.0254	8.659	2.559e-14
2	0.0381	0.0127	8.659	2.559e-14
3	0.0254	0.0127	2.165	2.559e-14
Case	**Fr (meas.)**	**Fr (pred.)**	**Fr (LBM)**	**Error (%)**
1	0.334	0.324	0.317	5.090
2	0.338	0.326	0.292	13.609
3	0.277	0.327	0.225	18.773

Figure 3 shows the capability of the model to capture the expected, non-axisymmetric shape profile of a Taylor bubble in an annulus. In the simulation, the bubble is initialised as an elongated, axisymmetric torus but naturally forms the minimal drag shape as observed in the figure.

Conclusions

The phase field lattice Boltzmann model has been used to analyse Taylor bubbles over an array of dimensionless parameters, for a range of inclination angles as well as in annular piping configurations. Where available, the terminal bubble velocity was shown to agree well with previous correlations, numerical data and experimental results. Looking forward, the dynamics of Taylor bubbles in annular piping geometries will be analysed. Additionally, a numerical database is being further generated to relate important dimensionless parameters to rise velocities and liquid film thicknesses to improve the reliability of mechanistic pressure gradient and liquid hold-up predictions.

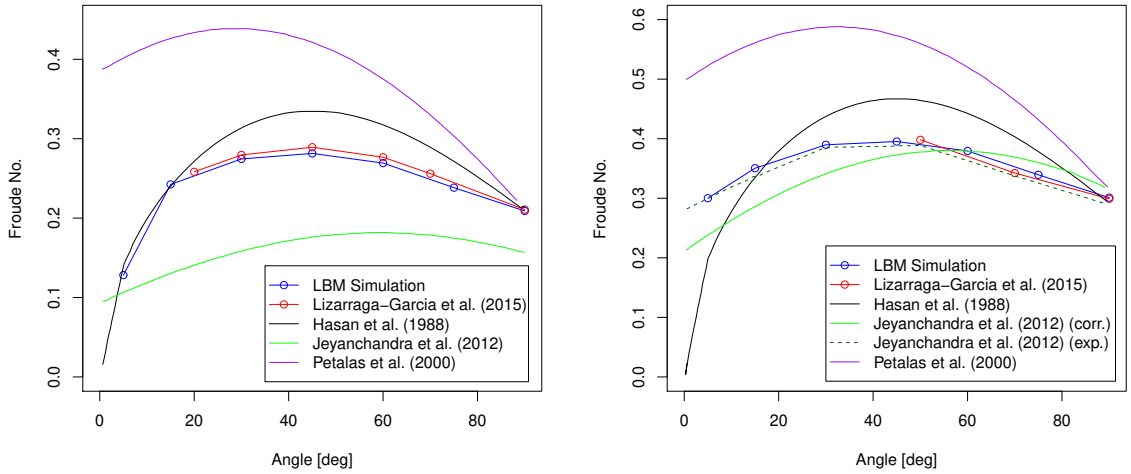

(a) Case A

(b) Case G

Figure 2: Froude number displayed as a function of inclination angle for test cases (a) A and (b) G. Case A is shown in comparison to existing correlations, while Case G is also compared with the experimental work of Jeyachandra *et al.* [7].

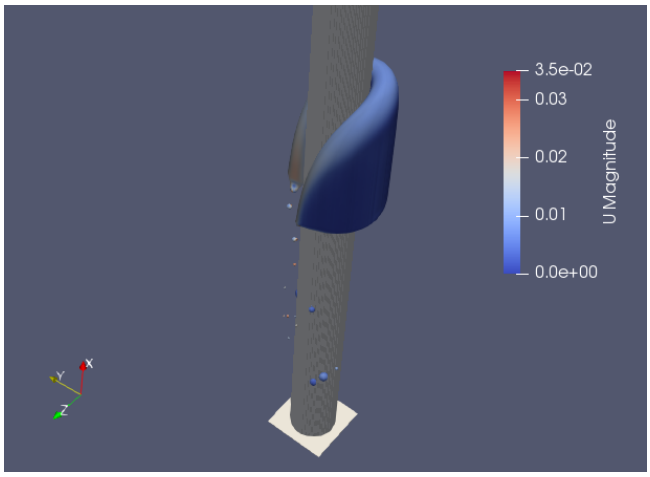

Figure 3: The vertical propagation of a Taylor bubble in an annular geometry. The contour indicates dimensionless velocity.

References

[1] Bugg, J. D. and Saad, G. A., The velocity field around a Taylor bubble rising in a stagnant viscous fluid: numerical and experimental results, *Int. J. Multiphase Flow*, **28**, 2002, 791–803.

[2] Chiu, P.-H. and Lin, Y.-T., A conservative phase field method for solving incompressible two-phase flows, *J. Comput. Phys.*, **230**, 2011, 185–204.

[3] Das, G., Das, P. K., Purohit, N. K. and Mitra, A. K., Rise velocity of a Taylor bubble through concentric annulus, *Chem. Eng. Sci.*, **53**, 1998, 977–993.

[4] Fakhari, A., Mitchell, T., Leonardi, C. and Bolster, D., Improved locality of the phase-field lattice Boltzmann model for immiscible fluids at high density ratios, *Phys. Rev. E*, **96**, 2017, 053301.

[5] Geier, M., Fakhari, A. and Lee, T., Conservative phase-field lattice Boltzmann model for interface tracking equation, *Phys. Rev. E*, **91**, 2015, 063309.

[6] Hasan, A. and Kabir, C., Predicting multiphase flow behavior in a deviated well, *SPEPE*, **3**, 1988, 474–482.

[7] Jeyachandra, B. C., Gokcal, B., Al-Sarkhi, A., Sarica, C. and Sharma, A., Drift-velocity closure relationships for slug two-phase high-viscosity oil flow in pipes, *SPE Journal*, **17**, 2012, 593–601.

[8] Lizarraga-Garcia, E., Buongiorno, J., Al-Safran, E. and Lakehal, D., A broadly-applicable unified closure relation for Taylor bubble rise velocity in pipes with stagnant liquid, *Int. J. Multiphase Flow*, **89**, 2017, 345–358.

[9] Llewellin, E. W., Bello, E. D., Taddeucci, J., Scarlato, P. and Lane, S. J., The thickness of the falling film of liquid around a Taylor bubble, *P. Roy. Soc. A-Math. Phy.*, **468**, 2012, 1041–1064.

[10] Mitchell, T., Leonardi, C. and Fakhari, A., Development of a three-dimensional phase-field lattice Boltzmann method for the study of immiscible fluids at high density ratios, *Int. J. Multiphase Flow*.

[11] Nogueira, S., Riethmuler, M. L., Campos, J. B. L. M. and Pinto, A. M. F. R., Flow in the nose region and annular film around a Taylor bubble rising through vertical columns of stagnant and flowing Newtonian liquids, *Chem. Eng. Sci.*, **61**, 2006, 845–857.

[12] Petalas, N. and Aziz, K., A mechanistic model for multiphase flow in pipes, *J. Can. Petrol. Technol.*, **39**.

[13] Shosho, C. E. and Ryan, M. E., An experimental study of the motion of long bubbles in inclined tubes, *Chem. Eng. Sci.*, **56**, 2001, 2191–2204.

[14] Viana, F., Pardo, P., Yanez, R., Trallero, J. L. and Joseph, D. D., Universal correlation for the rise velocity of long gas bubbles in round pipes, *J. Fluid Mech.*, **494**, 2003, 379–398.

[15] Wu, B., Firouzi, M., Mitchell, T., Rufford, T., Leonardi, C. and Towler, B., A critical review of flow maps for gas-liquid flows in vertical pipes and annuli, *Chem. Eng. J.*, **326**, 2017, 350–377.